Inverse lithography for 45-nm-node contact holes at 1.35 numerical aperture

Monica Laurel Kempsell
Rochester Institute of Technology
82 Lomb Memorial Drive
Rochester, New York 14623

Eric Hendrickx
IMEC
Kapeldreef 75
B-3001, Leuven
Belgium

Alexander Tritchkov
Kyohei Sakajiri
Mentor Graphics Corporation
8005 SW Boeckman Road
Wilsonville, Oregon 97070

Kenichi Yasui
Susuki Yoshitake
NuFlare Technology, Inc.
8 Shinsugita-cho, Isogo-ku
Yokohama-shi, Kanagawa, 235-0032
Japan

Yuri Granik
Mentor Graphics Corporation
8005 SW Boeckman Road
Wilsonville, Oregon 97070

Geert Vandenberghe
IMEC
Kapeldreef 75
B-3001, Leuven
Belgium

Bruce W. Smith
Rochester Institute of Technology
82 Lomb Memorial Drive
Rochester, New York 14623

Abstract. Inverse lithography technology (ILT) is a procedure that optimizes the mask layout to produce an image at the wafer with the targeted aerial image. For an illumination condition optimized for dense pitches, ILT inserts model-based subresolution assist features (AF) to improve the imaging of isolated features. ILT is ideal for random contact hole patterns, in which the AF are not at intuitive locations. The raw output of ILT consists of very complex smooth shapes that must be simplified for an acceptable mask write time. It is challenging for ILT to quickly converge to the ideal pattern as well as to simplify the pattern to one that can be manufactured quickly. ILT has many parameters that effect process latitude, background suppression, conversion run time, and mask write time. In this work, an optimization procedure is introduced to find the best tradeoff between image quality and run time or write time. A conversion run time reduction of 4.7× is realized with the outcome of this optimization procedure. Simulations of mask write time quantify the ability of ILT to be used for full chip applications. The optimization procedure is also applied to alternate mask technologies to reveal their advantages over commonly used 6% attenuated phase shift masks. © *2009 Society of Photo-Optical Instrumentation Engineers.* [DOI: 10.1117/1.3263702]

Subject terms: contact hole imaging; inverse lithography; model-based assist features; mask write time.

Paper 09067PR received Apr. 3, 2009; revised manuscript received Jul. 23, 2009; accepted for publication Oct. 2, 2009; published online Nov. 18, 2009. This paper is a revision of a paper presented at the SPIE conference on Optical Microlithography XXI, February 2008, San Jose, California. The paper presented there appears (unrefereed) in SPIE Proceedings Vol. 6924.

1 Introduction

The imaging of contact hole (CH) layouts is one of the most challenging tasks in hyper-NA lithography. Previous studies on CH imaging have shown that quadrupole or Quasar illumination is suited best to control the mask error enhancement factor (MEEF) at dense pitches, and thus provides the highest resolution.[1] The disadvantage of Quasar illumination is that it provides low depth of focus (DOF) and exposure latitude (EL) for the more isolated features. Fortunately, the EL and DOF for dark-field CH layouts can be enhanced by the use of subresolution assist features (AF). The insertion of AF in a design has previously been done using rule-based scripting. Developing a rule for AF placement is relatively straightforward for patterns that consist of long 1-D lines or spaces, but the complexity greatly increases when the pattern acquires periodicity in two directions, such as for regular CH arrays. For random CH arrays, writing a suitable rule for AF placement becomes an almost impossible task.

Inverse lithography is so named due to its approach to lithography in an inverse manner; instead of simulating the

1932-5150/2009/$25.00 © 2009 SPIE

Downloaded from SPIE Digital Library on 27 Jan 2010 to 129.21.240.32. Terms of Use: http://spiedl.org/terms

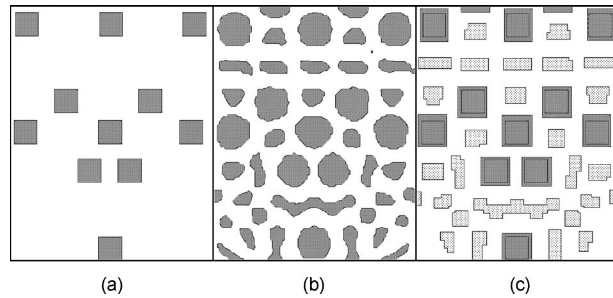

Fig. 1 (a) Target layout, (b) converted pattern, and (c) simplified pattern with OPC'd target features and inserted AF.

aerial image given mask features, it calculates required mask features given a target aerial image.[2] The Mentor Graphics (Wilsonville, Oregon) PIXbar inverse lithography routine was used to place model-based AF for a random CH clip drawn at a minimum pitch of 115 nm with Quasar illumination at 1.35 NA. This inverse lithography technology is a mask synthesis process that optimizes the mask shapes based on the optical image analysis for all image pixels in the work region. The mask synthesis is performed as a mathematical optimization process that minimizes a pixel-based objective function. Unlike pixel flipping, the pixels defined in PIXbar have continuous transmission values, which leads to a smoother and more meaningful convergence behavior. The analytical gradient, which is computed for all pixels, enables efficient quasi-Newton searching through the enormous solution space.[3] The mask synthesis process typically produces main feature shapes surrounded by subresolution AF shapes as well as, in some cases, negative AF inside the main feature shapes. To eliminate undesirable solutions such as printed AF, constrained optimization techniques are employed. This approach helps narrow down the solution space in a physically meaningful way, and improves the overall convergence behavior. The concept of mask equalization through high/low peak intensity leveling to achieve larger common process windows as well as some of the early experimental results of inverse lithography have been thoroughly discussed.[4–6]

Unsimplified optimization results of the design inversion contain polygons with lots of small features and arbitrarily angled edges. It is particularly problematic to have lots of small features that cause not only mask-writing inaccuracy but also can significantly increase the electron beam mask writer shot count. To address this issue, the simplification process takes the final design inversion result and turns it into a mask rule constraint (MRC) acceptable result while ensuring that resultant mask shapes will not cause undesirable imaging effects such as printing AF. The target, unsimplified conversion, and corresponding simplified pattern are shown in Fig. 1. How exactly such simplification should be performed, however, is somewhat of an open question due to complexities of the geometry with potentially conflicting conditions. In this work, simplification options are explored and analysis on the tradeoff between image quality and mask write time is provided.

In Sec. 2, the optimization procedure is discussed. The relationship of conversion parameters to image quality, conversion run time, and mask write time is determined,

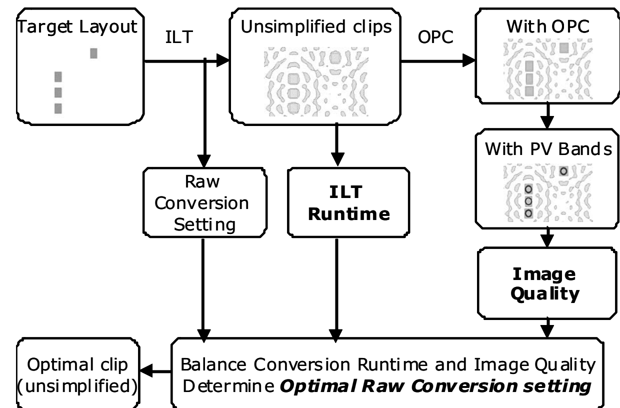

Fig. 2 Unsimplified conversion optimization procedure to select optimal settings with good image quality and fast conversion run time.

and optimal conversion settings for large process windows, fast conversion time, and fast mask write time are selected. In Sec. 3, experimental wafer data clearly show improved imaging of the random CH clip when treated with model-based AF and printed with Quasar illumination, compared to a clip with no AF. In Sec. 4, inverse lithography is extended to alternate mask technologies, and experimental data show improvement of 30% AttPSM over 6% AttPSM.

2 Theory and Simulation

There are several parameters to specify for both the conversion and simplification runs. For the initial conversion, the image-based parameters of target maximum intensity, target minimum intensity, optical model grid, kernels, and iterations must be specified. Each of these parameters can affect the image quality, the run time of the conversion, and the mask write time. A tradeoff between good image quality and fast run times is found. Fast conversion run times and mask write times are crucial for full chip applications due to the computational and throughput requirements for masks. Next, the optimization method is discussed that selects the best conversion parameter settings to balance image quality and run time, as well as selects the best simplification settings to balance image quality and mask write time.

2.1 *Optimization of Unsimplified Conversion*

A clip with 600 CH in multiple geometries with a target critical dimension (CD) of 70 nm and a densest pitch of 115 nm was run through PIXbar with Quasar illumination at 3240 unsimplified conversion settings, following the procedure in Fig. 2. The parameter values used within PIXbar are shown in Table 1, where the range of intensity values is {0,1}. Each converted clip was applied optical proximity correction (OPC) with Mentor Graphics OPCpro. The OPC settings were such that the image would print on target at best dose/best focus, and were kept constant throughout the procedure. Mentor Graphics OPCVerify was used to simulate process variation (PV) bands, MEEF, and background suppression (quantified as assist feature printing). A PV band is the inverse intersection of images taken through focus and dose. The smallest image is created out of focus with a small exposure dose, and the largest image is created

Downloaded from SPIE Digital Library on 27 Jan 2010 to 129.21.240.32. Terms of Use: http://spiedl.org/terms

Table 1 Conversion settings used to convert target layout into clips with unsimplified AF.

Pixbar parameter	Values							
Grid (nm)	6	8	10	15	20			
Iterations	30	40	50	60	70	80	90	100	120
Max intensity	0.5	0.6	0.7						
Min intensity	0	0.005	0.01	0.06					
Kernels	2	4	6	8	10	12			

in focus with a large dose, as shown in Fig. 3. Since the area of the PV band represents how much the image changes through focus and dose, it is inversely proportional to the process window. Thus, a decreasing PV band correlates to increasing image quality, so a minimal PV band is desired.[7]

PV bands were generated at ±60-nm defocus and ±10% dose for each of the 3240 clips. The areas of the PV bands for each CH were placed in bins according to their size, and this distribution is defined as the process variation band histogram. A comparison of the histograms for an unsimplified clip and a simplified clip to one treated with traditional OPC is shown in Fig. 4. Due to the narrower PV band areas, the figure clearly shows that the process window with unsimplified AF is much greater, and the simplified clip is also much improved over no AF. Within the histogram, contact holes with regular geometries, such as part of a regular array, have a smaller PV band area than contact holes with irregular geometries such as several contact holes on the diagonal.

The PV band areas of the 600 contact holes in each clip were averaged to quantify image quality for each correlated conversion setting, defined as average PV band area. The clips with unacceptable background suppression (one or more printed assist feature) were removed from the considered clips, such as those generated with an optical model grid of 20 nm. A graph of the calculated average PV band area versus the measured conversion run time is shown in Fig. 5. The calculated average MEEF versus conversion run time is shown in Fig. 6. Conversion settings that correlate to clips with a low PV band area, a low MEEF, and a relatively fast run time were selected, shown as the two circled clips.

All output clips were analyzed to determine the relationship of each PIXbar parameter to conversion run time, process window, MEEF, and background suppression. Evaluation of the optical model grid's relationship to the average PV band area can be seen in Fig. 5. The smallest grid results in the lowest PV band area but requires the longest conversion run time. The highest grid is the fastest to convert, but results in the highest PV band area, or worst process latitude. Thus, an increasing grid is correlated to an increase in average PV band area and a decrease in conversion run time.

The impact of number of iterations on average PV band area and conversion run time can be seen in Fig. 7. The lowest number of iterations results in the lowest PV band area and is the fastest to convert. The highest number of iterations results in the highest PV band area and takes the longest to convert. Thus, increasing iterations are correlated to a decrease in image quality and an increase in conversion run time. The finding that image quality decreases with iterations is counterintuitive. This correlation is due to the algorithm's background suppression effort, which improves with the number of iterations, shown in Fig. 7(c). A more effective background suppression results from smaller AF generated with a high number of iterations, but smaller AF do not improve the process window as much as larger AF. Thus, the tradeoff between process window and background suppression must be considered when selecting the number of iterations.

In analyzing the resulting MEEF values, it was found that as both grid and iterations increase, the value of MEEF also increases. This analysis was also performed for kernels, target maximum intensity, and target minimum inten-

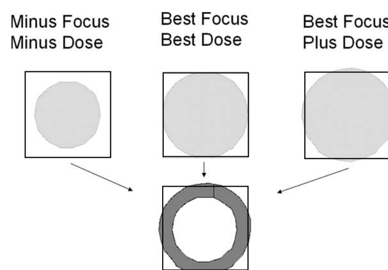

Fig. 3 Generation of PV band from images at multiple process conditions.

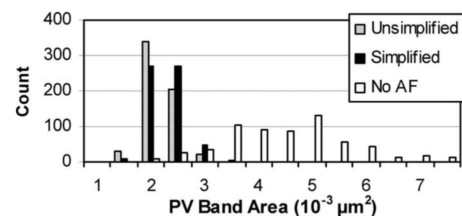

Fig. 4 PV band histograms of a clip with unsimplified AF, simplified AF, and no AF. The AF decrease the PV band area thus provide a higher process latitude. Image quality with simplified AF is slightly degraded over unsimplified, but is still a vast improvement over no AF.

Downloaded from SPIE Digital Library on 27 Jan 2010 to 129.21.240.32. Terms of Use: http://spiedl.org/terms

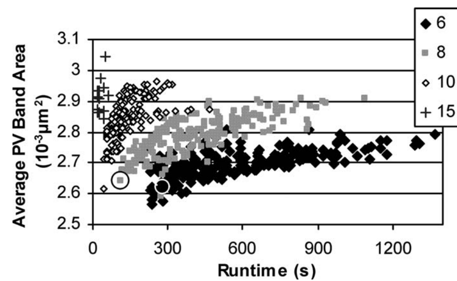

Fig. 5 A plot of average PV band area for each conversion setting versus conversion run time, filtered by grid. Smaller grid provides a lower PV band area thus higher image quality at the expense of long run times. Selected clip 1 is circled in black and selected clip 2 is circled in white.

Table 2 Two selected conversion settings compared to traditional settings.

Pixbar parameter	Traditional	Clip 1	Clip 2
Grid (nm)	6	8	6
Iterations	100	40	30
Max intensity	0.5	0.5	0.5
Min intensity	0.01	0.01	0.06
Kernels	6	4	10
Run time (CPU* hours)	14400	3060	

sity. It was found that increasing kernels led to increased run time, but not a significant improvement in image quality past four kernels. Increasing I_{max} led to no change in run time or MEEF and a slight degradation in image quality. Increasing I_{min} led to no change in run time or MEEF and a slight improvement in image quality. These conclusions led to the selected conversion settings listed in Table 2, which are circled in Figs. 5 and 6. Selected optimal conversion settings of clip 1 were used to convert a full chip layout with similar design characteristics as the random CH clip. As compared to traditional conversion settings used before the optimization procedure, PIXbar run time was reduced by a factor of 4.7.[6] This shows that when the settings are selected appropriately, inverse lithography has the capability to be useful for a full chip application.

2.2 *Optimization of Simplification Routine*

The two selected clips listed in Table 2 were run through a similar optimization procedure to select optimum simplification settings, shown in Fig. 8. The simplification settings for minimum area, width, space, and offset used in PIXbar are shown in Table 3. Each of the two clips was converted with 256 simplification settings, and simulations by NuFlare (Kanagawa, Japan) of a full field 104×132 mm mask (array of random CH clips) revealed the mask write time. Calculation of mask write time takes into account current density, maximum shot size, resist sensitivity, settling time of DAC amplifiers, field size, number of passes, and stage movement. Shot division is emulated by software in this calculation, and simulated write time corresponds to actual writing time within $\pm 10\%$ error. Calculation time takes less than one minute for a typical full field mask. The settings for a 50-keV EBM-6000 mask writer were used; a current density of $70\ \mathrm{A/cm^2}$ and maximum shot size of $0.8\ \mu\mathrm{m}$ square. The $7\text{-}\mu\mathrm{C/cm^2}$ sensitivity of a Fuji Film positive chemically amplified resist, FEP-171, was used for this two-pass mask write time calculation. Actual applied dose in each shot was adjusted by proximity correction to compensate for the additional dose from local pattern density. In these calculations, doses of $9\ \mu\mathrm{C/cm^2}$ were used on the assumption that the small clips had uniform pattern densities.

The average PV band area for each of the 256 output clips was calculated as image quality assessment. The rela-

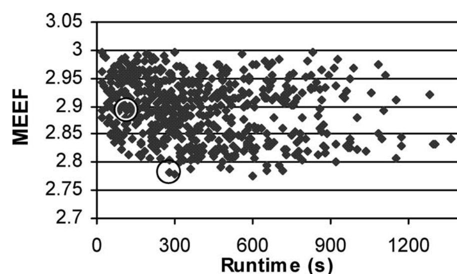

Fig. 6 A plot of the resulting MEEF for each conversion setting versus conversion run time. Selected clip 1 is circled in white and selected clip 2 is circled in black.

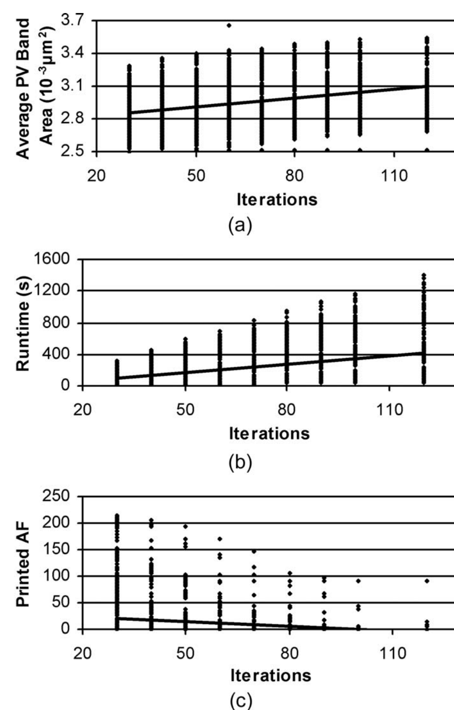

Fig. 7 Linear regression for (a) iterations versus average PV band area, (b) iterations versus conversion run time, and (c) iterations versus AF printing. The benefit of a high number of iterations is background printability control at the expense of high run time and slight image degradation.

Downloaded from SPIE Digital Library on 27 Jan 2010 to 129.21.240.32. Terms of Use: http://spiedl.org/terms

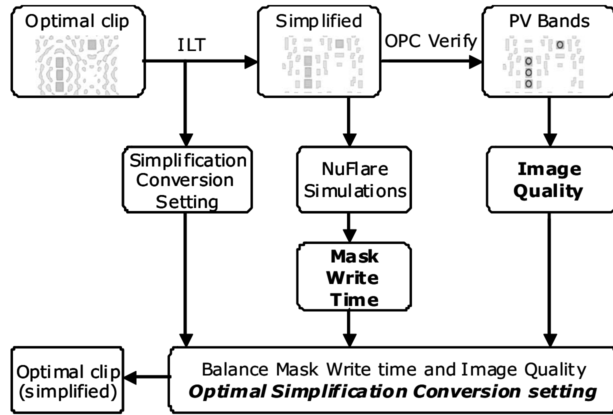

Fig. 8 Simplified conversion optimization procedure to select optimal simplification settings with good image quality and fast mask write time.

tionship between average PV band area and simulated mask write time, filtered by grid, is shown in Fig. 9. Grid 6 refers to simplification settings on selected clip 2, and grid 8 refers to selected clip 1. The maximum allowable mask write time is 12 h, shown as the dashed line. The relationship between MEEF and simulated mask write time, filtered by grid, is shown in Fig. 10. These figures reveal that for carefully selected simplification settings, the mask write time can be within the required 720 min with a minimal degradation of image quality. The relationship between the optical model grid and mask write time is evident; as the optical grid in the unsimplified conversion increases, the mask write time improves with a slight degradation in image quality.

Examination of the simulations show that some parameter settings provide a poor tradeoff between average PV band area and mask write time. When the minimum area is too large, the primary orthogonal AF can be removed during simplification, which proves detrimental to the image quality. This can be seen in Fig. 11(a), where the layout with minimum area of 3000 nm^2 results in numerous missing AF. The circled data points in Fig. 11(c) represent those generated with 3000 nm^2 that result in a poor tradeoff between mask write time and image quality. A similar relationship between MEEF and mask write time was found; if the minimum area is too large, the MEEF is much larger with no improvement in mask write time. Correlations with minimum space and minimum offset are much weaker (r^2 <0.1), but still show a slight deterioration in image quality with increasing simplification. These conclusions led to three simplification settings that compromise the tradeoff between mask write time and image quality, shown in Table 4, which are shown in Fig. 9 as the black data series in the 8-nm grid.

The outcome of the optimization procedure revealed that inverse lithography has the potential to be a full chip solution when both the initial conversion settings and simplification settings are selected appropriately. The usefulness of the technology also lies in the geometries in which inverse lithography has an advantage over rule-based AF insertion techniques. These geometries include nonregular arrays with diagonal geometries that are very complex for rule-based technologies. The advantage of inverse lithography over traditional OPC is examined in the following sections with experimental wafer measurements.

Table 3 Simplification settings used to simplify the model-based AF.

Pixbar simplification parameter	Values			
Min area (nm^2)	1500	2000	2500	3000
Min width (nm)	15	20	25	30
Min space (nm)	15	20	25	30
Min offset (nm)	15	20	25	30

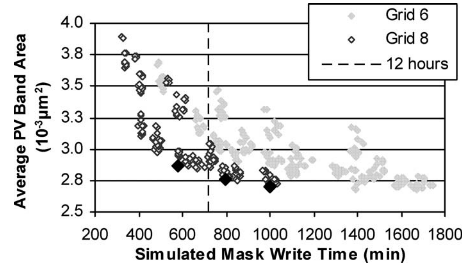

Fig. 9 Average PV band area versus simulated mask write time shows that image quality degrades at fast mask write times. Selected clips are shown as black data points, which are part of the 8-nm grid series and are listed in Table 4.

3 6% Attenuated Phase Shift Mask Experimental Data

The random CH array used in the optimization procedure was exposed for experimental validation. The mask was MoSi on Qz, where the MoSi was deposited at a thickness to enable 6% transmission, and both Qz and MoSi were partially etched to enable 180-deg phase shift. This mask also included arrays of varying contact CDs, pitch, and bias to evaluate CD uniformity (CDU) and MEEF. Doublets, triplets, and skewed arrays were also included to evaluate 2-D printing, background suppression, process windows, and MEEF in random environments. The 6% attenuated phase shift mask (AttPSM) was exposed on an ASML XT:1900i scanner (1.35 NA) with Quasar illumination of

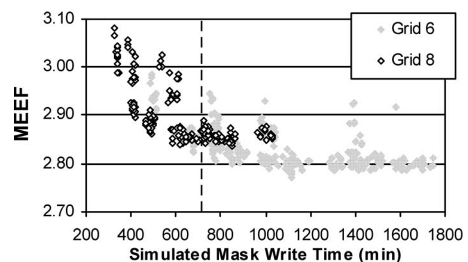

Fig. 10 MEEF versus simulated write time shows that better image quality can be reached with grid 6 at the expense of higher write times. The dashed line indicates 12 h.

Downloaded from SPIE Digital Library on 27 Jan 2010 to 129.21.240.32. Terms of Use: http://spiedl.org/terms

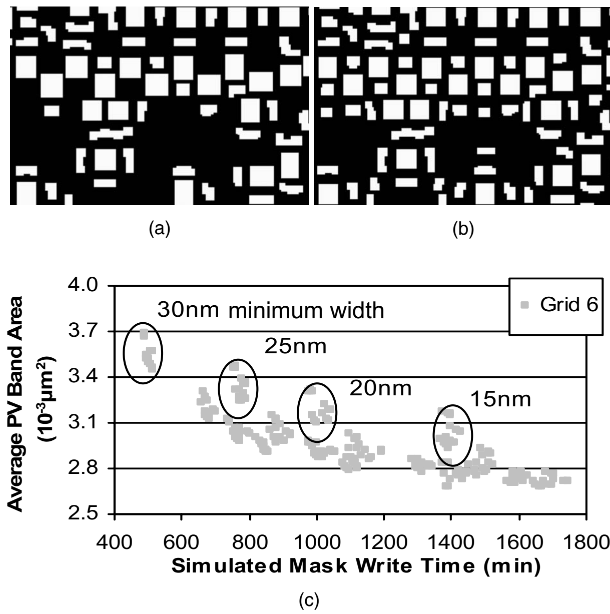

Fig. 11 Simplified mask patterns for (a) 3000-nm^2 minimum area and (b) 2500-nm^2 minimum area, which shows that when the minimum area is too large, necessary AF drop out. (c) Relationship between average PV band area and simulated mask write time for 6-nm grid. Circled regions indicate clips with 3000-nm^2 minimum area, which do not provide an acceptable tradeoff between image quality and mask write time.

30-deg opening angle and 0.93 to 0.69 outer-inner sigma. The resist process used 150-nm Sumitomo PAR823 on 77 nm of ARC29A. CD measurements were done on a KLA-T eCD2 using the CD2D algorithm and the process windows were analyzed in Klarity Prodata (KLA-Tencor, Milpitas, California) using a $\pm 10\%$ CD tolerance. As could be anticipated from simulation, there was a very strong performance improvement by using unsimplified AF over no AF.

Figure 12 shows the graphs with experimental maximal DOF and maximal EL for the CH indicated in the SEM picture. Regular and random CH geometries were selected to represent the different bins in the PV band histogram. Here a quantitative comparison can be made of the different CH configurations and the impact of the model-based assist features. It can be seen that the treatment without AF has the lowest EL and DOF, and that the isolated CH without AF has the lowest printability. For EL, all geometries show

Table 4 Three selected simplification settings.

Pixbar simplification parameter	Clip 1	Clip 2	Clip 3
Min area (nm^2)	2000	2000	2000
Min width (nm)	15	20	25
Min space (nm)	15	20	20
Min offset (nm)	15	20	20

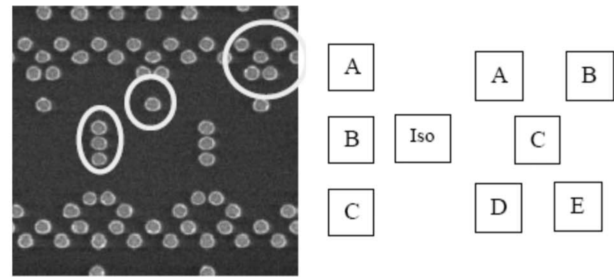

(a)

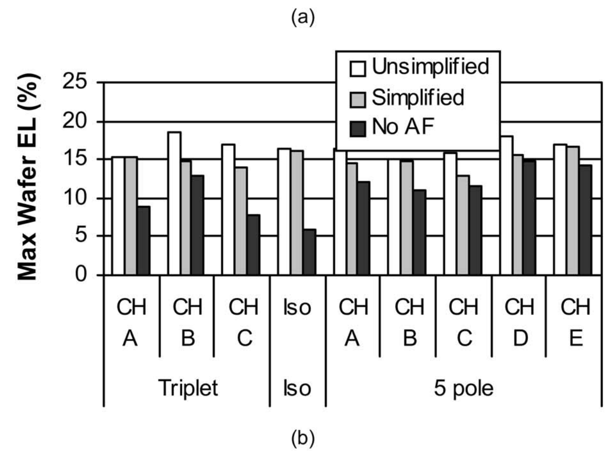

(b)

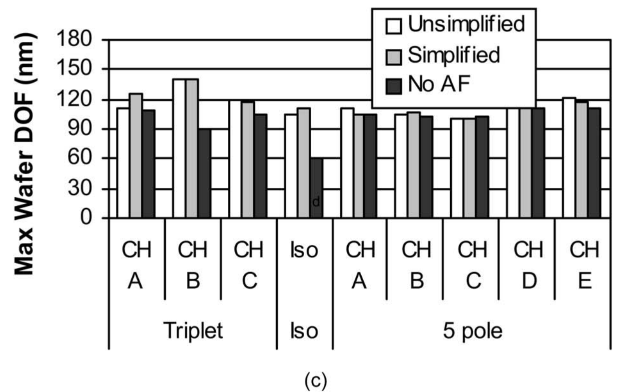

(c)

Fig. 12 (a) Geometries for which the process window was determined, and legend to the labels in the graphs. Experimental (b) maximum exposure latitudes and (c) maximum DOF for the CH in the different geometries.

a major improvement by placing unsimplified AF. When comparing the EL for simplified and unsimplified AF, one tendency that can be seen is that the unsimplified AF have slightly more EL than the simplified AF, or that simplification leads to some image degradation.[6]

4 Extension of Inverse Lithography Technology to Alternate Mask Technologies

4.1 *Optimization Routine for Alternate Technologies*

Alternate mask technologies such as alternating (Alt) PSM and high transmission attenuated PSM may offer a benefit in the image quality of CH patterns. Optimization routines as discussed in Sec. 2 were completed for these alternate masks. Figure 13 shows the smaller PV band area or larger process window that both 30% AttPSM and AltPSM have

Downloaded from SPIE Digital Library on 27 Jan 2010 to 129.21.240.32. Terms of Use: http://spiedl.org/terms

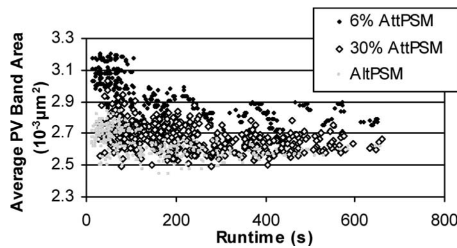

Fig. 13 Average PV band area for a traditional 6% AttPSM compared to the alternate mask technologies of 30% AttPSM and alternating PSM, before OPC. PV band area is smaller for the alternate technologies at comparable conversion run times, revealing higher process latitude.

over the traditional 6% AttPSM. Note that the PV band area was calculated with no applied OPC, which is why the 6% AttPSM PV band area values are larger than in Fig. 5.

4.2 *Theoretical Advantage of 30% over 6% Attenuated Phase Shift Masks*

The advantage of high transmission masks lies in the lower MEEF that can be obtained at dense pitches depending on mask bias, as shown in Fig. 14. The disadvantage when utilizing attenuated phase shift masks with high transmission is that various imaging problems occur due to the high background transmission. At intermediate pitches, the image can reverse and background printability must be controlled. The solution thus far has been to apply chrome to regions of undesired high intensity at wafer level to control background printing. The disadvantage of the combination of chrome with high transmission is that two patterning steps become critical in mask fabrication, increasing mask complexity.

Since the ILT algorithm targets maximum intensity inside the main CH as well as minimum intensity outside the main CH, this technique can convert a design for 30% AttPSM without using chrome in regions between the CH.[8] Chrome was only applied in regions that had received no AF and thus were far from the main CH. Thus, the benefit of the inverse lithography routine is to reduce the number of critical mask patterning steps from two to one. Analysis of converted designs shows that the AF are in positions similar to 6% AttPSM, but with increased size, as shown in Fig. 15. These larger AF will be easier to resolve during the mask making process.[9] The conversion and simplification optimization procedure discussed in Sec. 2 was performed for a 30% AttPSM with an identical target layout. Results

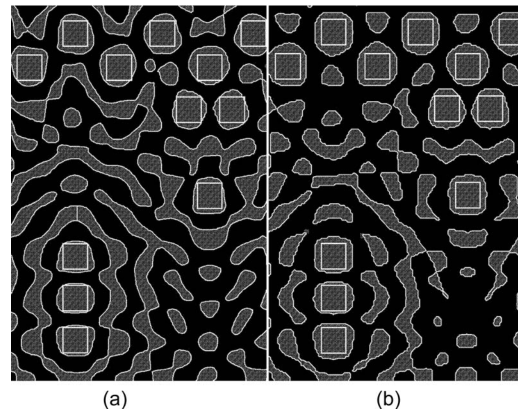

Fig. 15 ILT converted patterns with (a) 6% AttPSM and (b) 30% AttPSM. The squares are the targets and the curved shapes are ILT generated features. AF positions are similar, but sizes tend to be larger in the 30% case.

from these simulations after simplification confirm that the MEEF of 30% AttPSM is expected to be lower than that of 6% AttPSM, as shown in Fig. 16. The results also suggest that the process window may be enhanced by a high transmission PSM, shown in Fig. 13 as the lower average PV band area.

4.3 *Experimental Validation of 30% Attenuated Phase Shift Mask*

A 30% AttPSM with an identical target layout as the 6% AttPSM of Sec. 3 was exposed and measured with identical conditions for comparison. AIMS analysis and inspection on wafer confirmed the simulations, revealing good background suppression and pattern fidelity for the different geometries, as seen in Fig. 17.[9] MEEF was measured at three dense pitches near the resolution limit and was about 30% lower for 30% AttPSM, shown in Fig. 18, and so confirmed the simulated tendency. Wafer inspection revealed that isolated and semidense CH on 30% AttPSM with no AF did not print at all, revealing the importance of AF use for high transmission AttPSM.

The CD distribution of a 320-nm CH at 464-nm pitch on mask was found to have an 8 to 10-nm CD range, which is similar to what was observed on 6% AttPSM masks. Since MEEF for a 30% AttPSM is lower and the CDU on mask is similar to a 6% AttPSM, the CDU on wafer should improve for 30% AttPSM. The intrafield wafer CDU was measured for 116-nm pitch for a 6% and 30% AttPSM when the

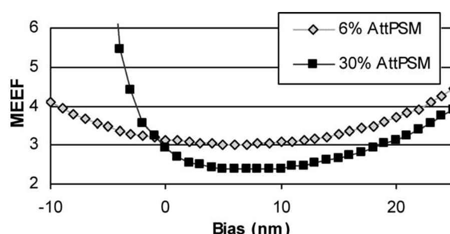

Fig. 14 Prolith simulation showing MEEF as a function of mask bias for 6% AttPSM and 30% AttPSM. At biases from 3 to 10 nm, 30% AttPSM provides a 20% reduction in MEEF.

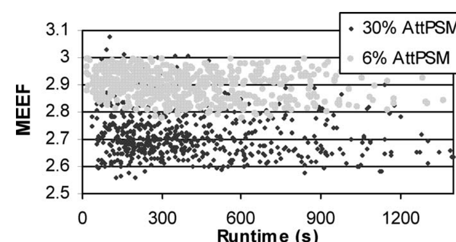

Fig. 16 Simulated MEEF versus conversion run time for simplified 6% and 30% AttPSM showing lower MEEF for 30% AttPSM.

Downloaded from SPIE Digital Library on 27 Jan 2010 to 129.21.240.32. Terms of Use: http://spiedl.org/terms

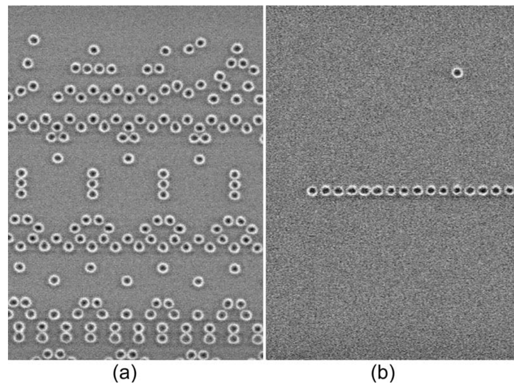

Fig. 17 The image of 30% AttPSM ILT converted patterns on a wafer exposed with ASML XT:1900i (1.35 NA, Quasar 0.93 to 0.69): (a) random CH with 115-nm minimum pitch and (b) CH on a line at 105-nm pitch showing good control of background printability.

masks were exposed back to back, shown in Fig. 19. The 30% AttPSM case shows significant improvement in measured CDU over the 6% case.

5 Conclusions

An optimization procedure is introduced to determine the ideal PIXbar conversion and simplification parameters that provide good image quality, fast conversion run time, and acceptable mask write time for 45-nm node CH. Image quality is quantified by PV bands, MEEF, and background printability. The relationship between each parameter to image quality, conversion run time, and mask write time is evaluated and optimal settings are recommended. The evaluated relationships recommend lowering the number of iterations and kernels from the previously used settings. Although the iterations are PIXbar specific, the fact that a limited number of kernels are successful in placing AF is a general conclusion that can be applied to any routine. Using the recommended settings, the conversion run time is reduced by a factor of 4.7, requiring 17 h with 180 CPU for full chip conversion. Mask write time simulations from NuFlare reveal that the minimum area parameter needs to be small for acceptable image quality, and that the minimum offset and minimum space parameters have little impact on write time and so can be kept small. Note that the minimum AF size and space between AF are crucial factors for every simplification routine. With these recommended simplification settings, full field mask write time can be reduced to 580 min.

Experimental data from a 6% AttPSM reveal a significant improvement in process latitude when going from no AF to unsimplified model-based AF. The process latitude degrades slightly with simplification, but still remains an improvement over no AF. The ILT treatment is also applied to alternate lithographic technologies including 30% AttPSM. Simulation and experimental data verify an improvement in MEEF and CDU when moving from 6% AttPSM to 30% AttPSM. Background printing, a concern for high transmission AttPSM, is successfully suppressed without a critical chrome patterning step using the PIXbar procedure. In summary, the developed optimization procedure reveals the potential for inverse lithography to be utilized in a full chip application and on alternate mask technologies.

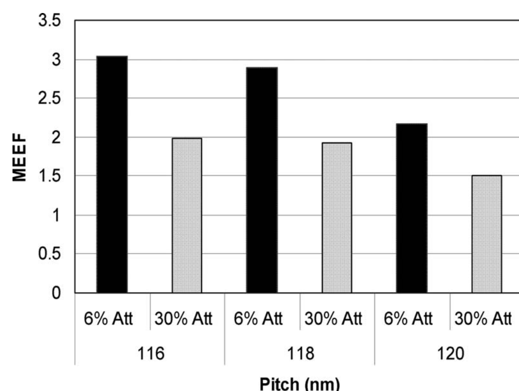

Fig. 18 MEEF measured on 70-nm CH with 16-nm bias for 6% AttPSM and 30% AttPSM reveals that MEEF is 30% lower for 30% AttPSM.

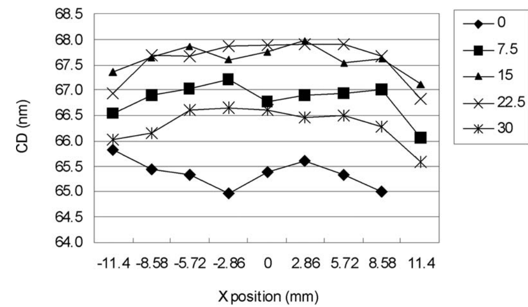

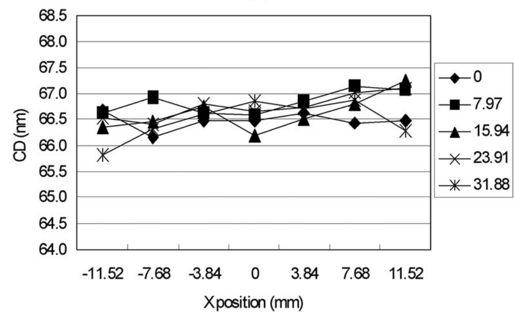

Fig. 19 Intrafield CDU measurements on 70-nm CH with 15-nm bias for (a) 6% AttPSM with range 3.0 nm and 3σ 2.7 nm, and (b) 30% AttPSM with range 1.2 nm and 3σ 0.9 nm.

Acknowledgments

The authors would like to thank the IMEC Advanced Lithography group as well as both of the reviewers for their thorough reading and helpful comments.

References

1. J. Bekaert, E. Hendrickx, and G. Vandenberghe, "60 nm half-pitch contact layer printing: exploring the limits at 1.35 NA lithography," *Proc. SPIE* **6924**, 69243A (2008).
2. Y. Granik, "Solving inverse problems of optical microlithography," *Proc. SPIE* **5754**, 506–526 (2005).
3. Y. Granik, "On the uniqueness of optical images and solutions of inverse lithographical problems," *J. Micro/Nanolith. MEMS MOEMS* **8**, 031405 (2009).
4. C. Y. Huang, Q. Liu, K. Sakajiri, S. D. Shang, and Y. Granik,

Downloaded from SPIE Digital Library on 27 Jan 2010 to 129.21.240.32. Terms of Use: http://spiedl.org/terms

"Model-based insertion of assist features using pixel inversion method: implementation in 65 nm node," *Proc. SPIE* **6283**, 62832Y (2006).
5. B. W. Smith and D. E. Ewbank, "OPC and image optimization using localized frequency analysis," *Proc. SPIE* **4691**, 148–157 (2002).
6. E. Hendrickx, A. Tritchkov, K. Sakajiri, Y. Granik, M. Kempsell, and G. Vandenberghe, "Hyper-NA imaging of 45 nm node random CH layouts using inverse lithography," *Proc. SPIE* **6924**, 69240L (2008).
7. S. Jayaram, A. Yehia, M. Bahnas, H. A. M. Omar, Z. Bozkus, and J. L. Sturtevant, "Automatic assist feature placement optimization based on process-variability reduction," *Proc. SPIE* **6730**, 67302E (2007).
8. K. Sakajiri, A. Tritchkov, and Y. Granik, "Model-based SRAF insertion through pixel-based mask optimization at 32 nm and beyond," *Proc. SPIE* **7028**, 702811 (2008).
9. K. Sakajiri, A. Tritchkov, Y. Granik, E. Hendrickx, G. Vandenberghe, M. Kempsell, G. Fenger, K. Boehm, and T. Scheruebl, "Application of pixel-based mask optimization technique for high transmission Attenuated PSM," *Proc. SPIE* **7275**, 72750X (2009).

Monica Laurel Kempsell graduated summa cum laude with a BS in electrical engineering from Oregon State University in 2007. She is now a microsystems engineering PhD student at Rochester Institute of Technology in the Nanolithography Research Labs. She spent one year as the Mentor Graphics assignee to IMEC during which she was involved in the presented research.

Eric Hendrickx graduated from the University of Leuven (Belgium) in 1996, and after that was a postdoctoral research scientist at the University of Leuven and the University of Arizona (Optical Sciences Center). He joined the lithography imaging group at IMEC in 2001, where he currently is working on EUV lithography.

Alexander Tritchkov graduated from the Sofia University of Technology in 1987 with a MSc degree in semiconductor science and technology, specializing in microlithography. His work experience has focused on resolution and process window enhancement since 1994, with particular interests in models, algorithms, and software for proximity correction, subresolution assisting features (SRAFs), PSM, DFM, and simulation of advanced optical imaging systems and processes. Since 2007 he has been working on advanced RET at Mentor Graphics Corporation. His main focus is on solutions for mask optimization techniques (pixel-inversion technology) for various mask types, (6 and 30% attenuation, two- and three-tone AltPSM) for random and memory circuits, source optimization and source and mask optimization, and double patterning.

Kyohei Sakajiri is a software engineer at Mentor Graphics Corporation. He has several years of experience in research and development in areas related to resolution enhancement technologies as well as inverse lithography, and has authored or coauthored several papers on the topic of inverse lithography.

Susuki Yoshitake received the BS and MS degrees in material science and technology from Kyushu University, Fukuoka, Japan, in 1988 and 1990, respectively. He is the chief specialist working on the design and development of EB mask writers for next-generation lithography technology. He has more than 19 years experience in the semiconductor industry working at the Toshiba Research and Development Center, Toshiba Machine Company, Limited, and NuFlare Technology, Incorporated.

Kenichi Yasui received his BS degree in material science from Shimane University in 2004, and his MS degree in physics from Nagoya University in 2006, respectively. Since he joined NuFlare Technology, Incorporated, in 2006, he has worked on data preparation technology for the latest EB mask writers. His current focus is the development of viewing software for EB data prepared with CAD tools supplied by EDA benders.

Yuri Granik received his MS in AM/CS and PhD degree in theoretical physics from Odessa State University, Ukraine. From 1984 to 1991, he was a professor of applied mathematics in Odessa State University. He taught courses in mechanics, gas dynamics, hydrodynamics, and computer science. In 1991 he joined Technology Modeling Associates, Incorporated. As a project manager, he worked on TCAD tools, simulators, and integration frameworks, including lithography simulator DEPICT, parasitic extractor RAFAEL, and milestone IC technology workbenchs CAESAR, TWB, and DFM. In 1997 to 1998 he managed IC manufacturing data analysis projects at PDF Solutions, Incorporated. He is currently a technical leader for the process and OPC simulations and modeling in the Calibre division of Mentor Graphics Corporation. He has published more than 100 papers in the areas of hydrodynamics, technology CAD, and microlithography. He is Senior IEEE and SPIE member.

Geert Vandenberghe received his MS and PhD degrees from the Katholieke Universiteit of Leuven in Belgium. In 1995 he joined the lithography department at IMEC, where he has been working on resists, imaging, OPC, and resolution enhancement techniques. He is currently managing the reticle and imaging group of the lithography department and is program manager of the advanced lithography research program at IMEC.

Bruce W. Smith is the Intel Professor and Director of Microsystems Engineering at the Rochester Institute of Technology, where he has been involved with teaching and research in microlithography, thin films, optics, materials, and nanopatterning for more than 20 years. He received his PhD degree from RIT and has worked with various groups and organizations including Sematech and IMEC. He has published more than 100 technical papers and several textbook chapters and holds more than 20 patents. He is a fellow of SPIE and a member of OSA, IEEE, and AVS.

Downloaded from SPIE Digital Library on 27 Jan 2010 to 129.21.240.32. Terms of Use: http://spiedl.org/terms